Proceedings of International Conference on Heat Exchanger Fouling and Cleaning - 2013 (Peer-reviewed)
June 09 - 14, 2013, Budapest, Hungary
Editors: M.R. Malayeri, H. Müller-Steinhagen and A.P. Watkinson
Published online
www.heatexchanger-fouling.com

WHEN IS FOULING TOO FAST TO MEASURE THERMALLY?

V.Y. Lister[1,*], J.F. Davidson[1] and D.I. Wilson[1]

[1] Department of Chemical Engineering and Biotechnology, University of Cambridge, New Museums Site, Pembroke Street, Cambridge CB2 3RA, UK.

*E-mail: vyl20@cam.ac.uk

ABSTRACT

Many fouling tests employ an analysis of the change in heat transfer and thermal resistance to monitor fouling quantitatively. This approach is based on the assumption of momentary steady state. A mathematical analysis considering the validity of this steady state approach is described for three sets of boundary conditions commonly employed in fouling tests, and criteria for when the results are reliable are presented. An example of how ageing can affect the validity of the steady state approach is also presented. A short survey of experimental studies of fouling presented in the literature shows that gas-side particulate fouling is likely to contravene the reliability criteria, indicating that non-thermal methods should be used to study this phenomenon.

INTRODUCTION

Accurate measurement of fouling layer growth with time is important for both academic studies, such as investigating fouling mechanisms, and for industrial practice, such as determining the extent of fouling and elucidating process problems. One experimental methodology in common use is to monitor heat transfer performance and relate the change in overall heat transfer coefficient, U, to the thermal resistance of the fouling layer, R_f, via

$$R_f = \frac{1}{U(t)} - \frac{1}{U_{clean}} \qquad (1)$$

The R_f value can be related to the thickness of the fouling layer, a, by assuming that the system is momentarily at thermal steady state and that heat transfer across the layer occurs by conduction. For deposits which can be treated as a slab (flat surfaces, thin layers on curved surfaces, uniform deposition), R_f is related to a by

$$R_f = \frac{a}{k} \qquad (2)$$

where k is the thermal conductivity of the deposit material, which is assumed to be constant. The principle underlying this approach is that k is sufficiently low that the presence of a fouling layer creates a significant insulating effect, sufficient to monitor its presence.

The above analysis relies on the temperature profiles within the fouling layers being at steady state. This steady-state assumption implies that the temperature profiles through the fouling layer are linear and that the heat flux through the layer is constant (in planar co-ordinates). The steady state requirement implies that the timescale for heat transfer through the layer must be much faster than the timescale for layer growth. Fouling layers are usually insulating, however – this is why they cause problems - and the validity of the assumption of steady state should be confirmed. If the ratio of the timescales approaches unity the thermal resistances inferred from such measurements will be subject to systematic errors which could be large.

It is important to be able to anticipate cases where the validity of the above steady state approach (labelled SSA) is compromised. This paper presents results from a recent paper (Lister *et al*., 2012) where the validity of the SSA was subjected to a rigorous evaluation. The analysis yields criteria describing the parameter space in which the SSA is reliable. A series of experimental fouling studies reported in the literature covering the range of fouling mechanisms reported by Epstein (1983; crystallization, particulate, corrosion, chemical reaction and biofouling) are assessed against these criteria to establish which, if any, mechanisms are likely to violate the SSA and therefore require particular care when designing or interpreting experiments.

Epstein (1983) also highlighted the importance of ageing in fouling mechanisms and the interpretation of fouling data. Ageing here is manifested in a change of deposit thermal conductivity, which will change the relationship between thickness and R_f (Equation [2]). The analysis of Lister *et al*. (2012) is extended here to consider the validity of the SSA to interpret thermal measurements for deposits subject to ageing. The growth of aged material, with thermal conductivity different to that of freshly deposited material, is modelled using the two-layer ageing model presented by Ishiyama *et al*. (2011). A similar mathematical framework is employed to determine when the

growth of the aged layer is likely to introduce significant errors into the interpretation of heat transfer measurements.

THEORY

Fast Deposition

Figure 1 shows a fouling layer of thickness, $a(t)$, attached to a pipe wall and in contact with a warm process stream. The temperature difference between the stream and the wall drives heat flow through the deposit. The temperatures can be written in terms of a dimensionless temperature, θ, ranging from 0 to 1, *viz.*

$$\theta = \frac{T - T_{wall}}{T_a - T_{wall}} \tag{3}$$

Here T_{wall} and T_{a} are the temperatures at the wall-deposit interface and deposit-stream interfaces, respectively. The direction of heat flow (hot or cold wall) is not important to the analysis: a cold wall is used for convenience.

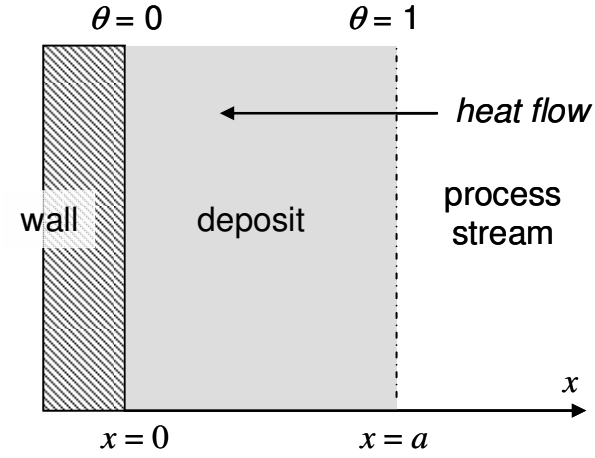

Fig. 1 Schematic of a deposit layer of thickness a growing on a cold wall.

The standard approach to determine the thermal resistance in experimental studies is to measure the heat flow and temperature difference ($T_{\text{a}} - T_{\text{wall}}$), calculate U and estimate R_{f} from Equation [1]. The deposit thickness is then inferred from R_{f} using Equation [2]. These relationships are derived by considering the one-dimensional heat-diffusion equation (Equation [4]) and taking the steady state limit.

$$\frac{\partial \theta}{\partial t} = \alpha \frac{\partial^2 \theta}{\partial x^2} \tag{4}$$

where α is the thermal diffusivity of the deposit layer. This relies on two key assumptions: the first is that the heat flux is constant and uniform through the layer, and the second is that this gives a linear temperature profile across the deposit.

The validity of the SSA can be quantified by writing the general solution to equation [4] (the heat diffusion equation) as:

$$\theta(x,t) = \theta^S(x,t) + \theta^T(x,t) \tag{5}$$

where $\theta(x,t)$ is the dimensionless temperature profile in the deposit at position x at time t. Superscripts S and T refer to the steady state profile and a transient deviation, respectively. The steady state profile is the linear profile in the SSA. A solution for θ^T can then be identified by considering a series of order of magnitude estimations. Their derivation is detailed in Lister *et al*. (2012). The form of θ^T dictates the magnitude of the error in the SSA.

The boundary conditions to be applied in solving Equation [4] are determined by the experimental technique. Three different cases are considered here:

I. *Constant temperature difference*
The temperatures at the wall-deposit interface and the deposit-process stream interface are constant. This could arise if phase changes (*e.g*. condensation, boiling) occur at these boundaries, or if the film heat transfer coefficients are very large, so that negligible temperature difference is required to drive the heat flow in the regions beyond the fouling layer.

II. *Constant heat flux*
An example of where this would arise is with a hot wall, with heat supplied at constant power. The process stream is at constant temperature (large film heat transfer coefficient).

III. *Finite film heat transfer coefficient*
Both the wall and the bulk process stream are at fixed temperature, but the film heat transfer coefficient for the latter, h, is finite, leading to T_{a} varying with time.

Each of these cases has different practical applications and all are applicable to various experimental apparatuses and industrial systems. For instance, Case II is an approximate description of experimental fouling probes based on electrical heating elements.

From the solutions to [4] one can estimate the error associated with using the steady state solution alone. Let the maximum acceptable error be 10%, such that:

$$\frac{\Delta a}{a} = \frac{a - a_{est}}{a} < 0.1 \tag{6}$$

where the estimated value of the fouling layer thickness, a_{est}, is calculated using the assumption of a linear temperature profile and constant heat flux. The linear temperature profile is used to extrapolate to the estimated thickness. One can then investigate magnitudes of the growth rate, $G = \text{d}a/\text{d}t$, at which such large errors arise.

Ageing

Ageing in this context is where the thermal conductivity of the foulant varies over time as a result of changes in the material's microstructure caused by physical or chemical reaction. Ageing is a complex phenomenon and reliable, quantitative descriptions of microstructure evolution and heat transfer have yet to be developed. In their absence, the simplified approach presented Ishiyama *et al.* (2010; 2011) is used here. Ageing is described by a two-layer model,

where the deposit is treated as consisting of layers of different thermal conductivities, here labelled 'coke' and 'gel' (see Figure 2). The gel is the freshly deposited material and the coke its aged form: the coke has a higher thermal conductivity than the gel and so as gel converts to coke the thermal resistance of the layer decreases. The thickness of the coke layer at time t is $b(t)$.

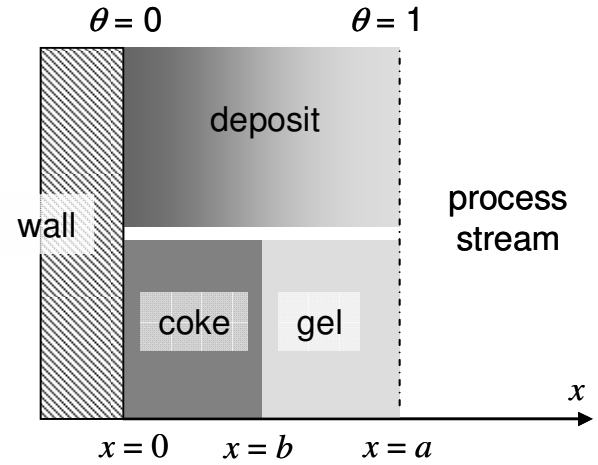

Fig. 2 Schematic of the two-layer model used to describe deposit ageing.

This system can be considered as two fouling layers growing with different growth rates and thermal conductivities. The temperature variables within the gel and coke layers are T_{gel} and T_{coke}, respectively. The governing equations and boundary conditions of the system are then:

Heat diffusion

$$\frac{\partial T_{coke}}{\partial t} = \alpha_{coke} \frac{\partial^2 T_{coke}}{\partial x^2} \qquad 0 \le x \le b \qquad (6)$$

$$\frac{\partial T_{gel}}{\partial t} = \alpha_{gel} \frac{\partial^2 T_{gel}}{\partial x^2} \qquad b \le x \le a \qquad (7)$$

Boundary conditions

$$T_{coke}(t, x = 0) = T_{wall} \qquad (8)$$

$$T_{coke}(t, x = b) = T_{gel}(t, x = b) \qquad (9)$$

$$k_{coke} \frac{\partial T_{coke}(t, x = b)}{\partial x} = k_{gel} \frac{\partial T_{gel}(t, x = b)}{\partial x} \qquad (10)$$

$$T_{gel}(t, x = a) = T_a \qquad (11)$$

Case I only is considered here, where the temperature difference across the composite fouling layer is fixed (Equations [8] and [9]). The position of the boundary between the two layers, b, and the overall thickness, a, both vary with time. The layers are assumed to have equal density so that ageing does not cause swelling or shrinkage.

The steady state solution for Equations [8-11] is linear in x, with the temperature gradient in each sub-layer inversely proportional to its thermal conductivity. The error associated with the SSA can be calculated as before by substituting a solution of the form of Equation [5] into the governing equations. The deviation between the SSA and true temperature profiles can then be calculated as a function of time.

RESULTS

Fast fouling, no ageing

Figure 3 shows the steady state and true profiles calculated for a fouling layer with Case I boundary conditions. The true profile clearly differs from the linear steady state profile. The difference arises from the finite volumetric heat capacity of the fouling layer, which causes some of the energy entering the deposit from the process stream to be stored in the fouling layer.

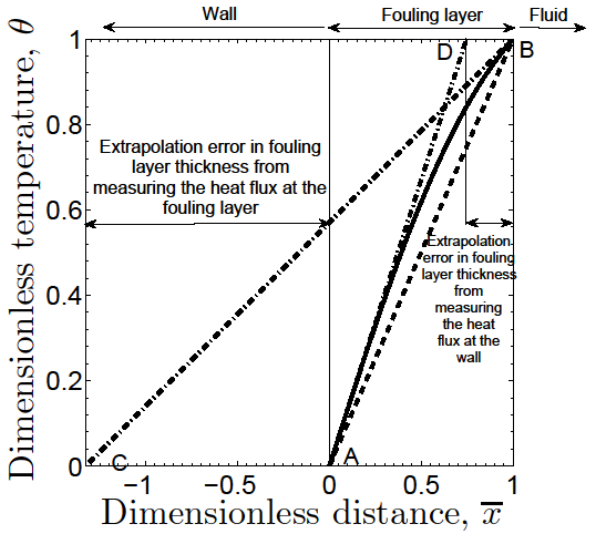

Fig. 3 Schematic illustrating the extrapolation errors involved in using the SSA when the temperature difference across the deposit layer is fixed (Case I) for a fouling layer with G =10^{-6} m/s and α = 10^{-6} m^2/s. The ordinate parameter is the scaled distance into the deposit layer, $\bar{x} = x/a$. The solid black line indicates the true profile and the dashed black line (AB) shows the steady state profile. The dash-dot lines show the gradients (AD and BC) and the error associated with the SSA. Reproduced from Lister *et al*. (2012)

The Figure also shows the extrapolation error when the fouling layer thickness is calculated using the SSA. In a typical experiment, the heat flux is monitored at the wall (x = 0) using a heat flux sensor. As the heat flux is assumed to be constant and uniform through the fouling layer, the temperature gradient can then be calculated and extrapolated to find the thickness of the fouling layer (line AD on the Figure).

The temperature gradient in the true profile (solid curve AB) is not, however, uniform and this extrapolation will yield the error shown in Fig. 3. The magnitude of the errors (DB and AC) depend on the thermal diffusivity of the fouling layer as this quantifies the ratio of heat being transferred through the layer to the heat being stored within the layer. As the thermal diffusivity of the fouling layer is finite, some of the heat is stored within the layer and gives a

curved temperature profile. The deviation increases in magnitude for faster growing fouling layers as the fouling layer stores more heat.

Figure 4 depicts a Case II example, where the heat flux to the layer, delivered through the wall, is fixed. As described above this corresponds where a device supplies heat at a constant flux to one side of the fouling layer. There is again a notable difference between the steady state and true profiles. The two have the same gradient at the wall (x = 0) as this is set by the heater but the SSA requires this to be uniform across the layer. The gradient in the true profile decreases with distance because of heat accumulating in the layer rather than being conducted through instantly.

The steady state profile also predicts a greater temperature difference than the true profile (in this case the wall temperature is not fixed and θ is scaled by the maximum temperature in the layer during the study). This is because the SSA method assumes that the layer has had a long time to accumulate heat and therefore reach a higher temperature. The error in thickness, AC, is again significant. The deviation increases in magnitude for faster growing layers (large G) and for layers with lower thermal diffusivities.

Applying the criterion in Equation [6] to the solutions for θ^{Γ} yields a series of criteria for when the SSA method is valid. Those obtained for non-ageing deposits (Cases I-III) are summarised in Table 1 and identify the key parameters which determine the error. These criteria are compared in Figure 5 for a range of thermal diffusivities and fouling growth rates representative of foulant materials and deposition rates. The Figure shows that the growth rate at which the error becomes significant depends strongly on the thermal diffusivity of the foulant (and, for Case III, on H). For materials with $\alpha \sim 10^{-7}$ m^2/s, *i.e.* oils and aqueous solutions, significant errors can arise when the growth rate is greater than 10^{-5} m/s (10 μm/s). The magnitude of the error depends on the boundary conditions (which Case). The effect is not significant at smaller growth rates, particularly in comparison with other errors involved in determining heat transfer coefficients.

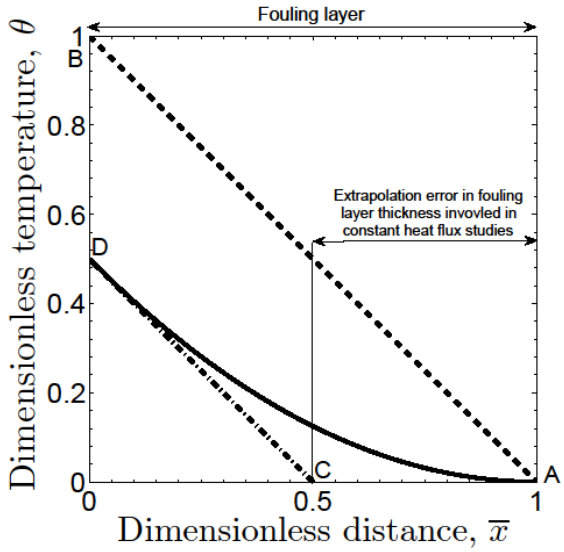

Fig. 4 Schematic illustrating the extrapolation error in the SSA approach for Case II (fixed wall heat flux) for a fouling layer with G = 10^{-6} m/s, α = 10^{-6} m^2/s. AD (solid line) is the true profile; AB the steady state profile. Reproduced from Lister et *al*. (2012).

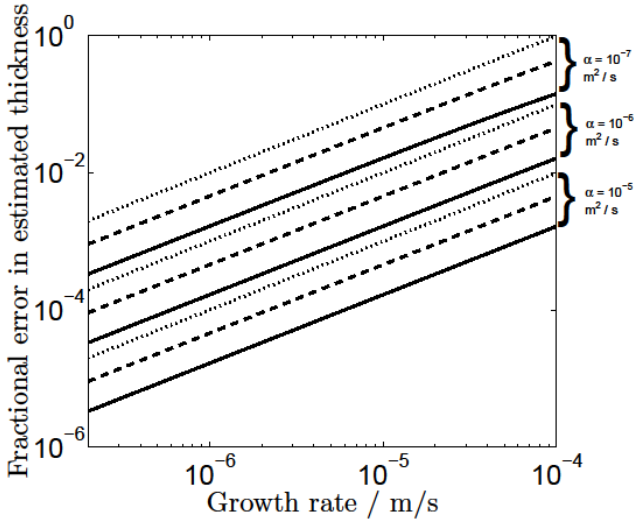

Fig. 5 Effect of fouling layer growth rate on the error in estimated deposit thickness when $H = h/k$ = 150 m^{-1}. No deposit ageing. Solid line – Case I; dotted line – Case II; dashed line – Case III (Table 1). Note log scales on both axes. Reproduced from Lister *et al*. (2012).

Table 1. Summary of the criteria for the SSA method to be valid (after Lister *et al*., 2012).

Case	Criterion
I. *Constant temperature difference*	$0.1 > \dfrac{1}{1+\dfrac{6\alpha}{aG}}$
II. *Constant heat flux*	$0.1 > \dfrac{da}{dt}\dfrac{a}{2\alpha}$
III. *Finite film heat transfer coefficient,* $H = h/k$	$0.1 > \dfrac{a\left(3+4a(H)+a^2H^2\right)\left(GH^2-k\right)}{H\left(a^3\left(GH^3-HdH/dt\right)+6H\alpha+12aH^2\alpha+3a^2GH^2-dH/dt+2H^3\alpha\right)}$

Fast fouling with ageing

Ageing introduces a second set of material properties and a second growth rate (via the ageing kinetics). A case study is presented here to illustrate the effect of ageing on heat transfer in a fast growing fouling layer. Whereas the previous analysis assumed a constant growth rate, more interesting results are obtained with falling rate fouling (and ageing) behaviour, which is typical of fouling under conditions of constant temperature difference (see Ishiyama *et al*. (2011)).

Figure 6 shows the temperature profiles obtained for a deposit subject to this ageing with coke and gel thermal conductivities (and thermal diffusivities) in the ratio 5:1 for Case I heat transfer conditions. The thickness of the whole deposit layer, $a(t)$, and the thickness of the aged layer, $b(t)$, are modelled as:

$$a(t) = g_D t^{0.5} \tag{12}$$

$$b(t) = g_A t^{0.65} \tag{13}$$

with parameters g_D = 9 μm/s$^{0.5}$ and g_A = 5 μm/s$^{0.65}$. These parameters gave noticeable effects for the case where k_{gel} = 0.1 W/m K and k_{coke} = 0.5 W/m K (typical values employed by Ishiyama *et al*. (2011)). For fast ageing, $g_A \sim g_D$, the problem approaches that of temperature transients in the coke layer, which have a short characteristic time owing to the higher thermal conductivity. For slow ageing, $g_A \ll g_D$, the problem collapses to the transient through the gel layer. The aged material has a higher thermal conductivity so the temperature gradient in the coke is smaller than that in the gel.

As with Figure 3, the true temperature profiles are noticeably different from the steady state results, owing to energy accumulation in the layers. The true temperature gradient in the coke at the wall is larger than the SSA value, while the gradient in the gel at the deposit-stream interface is smaller.

Criteria indicating conditions where the SSA can be taken to be valid, similar to those reported in Table 1, can be derived using a similar approach. The results are more complex and require knowledge of ageing rates which are not yet readily available.

A note on Kern-Seaton behaviour

The above findings have particular importance for fouling processes which exhibit falling rate behaviour. We analyse fouling behaviour which can be described by the Kern-Seaton (1959) model, *i.e*. rapid initial growth followed by an asymptotic approach to a limiting thermal resistance, $R_{f\infty}$. This model is widely used to quantify fouling behaviour even though it contains several simplifying assumptions (such as ignoring the effect of changing surface temperature as deposition proceeds), and is used here for illustration.

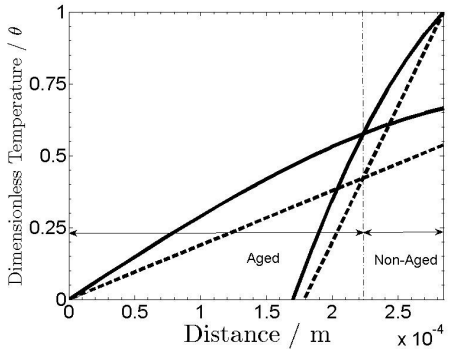

Fig. 6 Schematic illustrating the extrapolation error involved in using the steady-state fouling analysis approach to a deposit subject to ageing, with coke near the wall and gel as fresh deposit. Case I – fixed temperature difference. The dashed line shows the SSA temperature profile while the solid lines show the true profile. The central vertical line marks *b*, the boundary between the layers. The temperature scale is not normalised in this case. The growth rate of the fresh deposit at this instant was 14 μm/s and the ageing rate was 15 μm/s.

The Kern-Seaton model is based on competing deposition and removal steps, *viz*.

$$\frac{dR_f}{dt} = m_d - n_r R_f \tag{14}$$

with $R_{f\infty}$ given by

$$R_{f\infty} = m_d / n_r \tag{15}$$

The asymptotic fouling resistance is measured after long times and is a steady state parameter which is free from transient effects. Separating m_d and n_r via Equation [14], however, requires measurement of m_d, the initial fouling rate, *i.e*. when R_f = 0 m^{2}K/W. This is, however, also when the largest growth rate is observed and is thus most susceptible to errors associated with thermal transients.

SURVEY OF FOULING TYPES

In this section the results reported above are applied to several reported studies in the fouling literature to determine whether SSA errors are likely to arise in thermal fouling measurements on such systems. Where the analysis indicates that thermal measurements are likely to be subject to these transient effects, the challenge in those areas is to develop non-thermal methods for measuring growth rates.

A series of papers were selected, covering the five classes in Epstein's (1983) fouling characterisation schema. The papers and results are summarised in Table 2. A typical growth rate was identified, in the majority of cases from initial rate data, as these are normally when deposition is fastest (as with Kern-Seaton behaviour).

Table 2 Reported studies of fouling layer growth rates and thermal diffusivities for a range of fouling mechanisms.

Authors	Fouling type	Foulant material	Measurement method	Typical G (m/s)	Typical α (m^2/s)
Mahato *et al.* (1980)	Corrosion	Aluminium	Volume measurement	10^{-9}	$\times 10^{-5}$
Griess *et al.* (1964)	Corrosion	Steel	Direct measurement	10^{-11}	$\times 10^{-5}$
Characklis (1981)	Biofouling	Biofilms	Volumetric displacement	10^{-9}	$\times 10^{-7}$
Salley *et al.* (2012	Biofouling	*Synechococcus*	Fluid dynamic gauging	10^{-10}	$\times 10^{-7}$
Taylor (1969)	Chemical reaction	Decane	Mass measurement	10^{-11}	$\times 10^{-7}$
S. Subbarao *et al.* (2011)	Particulate	Ash	Optical	10^{-5}	$\times 10^{-7}$
Kalisz *et al.* (2005)	Particulate	Soot	Measurement of height	10^{-6}	$\times 10^{-7}$
Hasson *et al.* (1970)	Crystallisation	Calcium sulphate	Deposit mass measured	10^{-9}	$\times 10^{-6}$
Groberichter *et al.* (2003)	Crystallisation	Sodium chloride	Deposit mass measured	10^{-6}	$\times 10^{-6}$
Huang *et al*. (2011)	Crystallisation	Tripalmitin	Thermal measurement	10^{-7}	$\times 10^{-7}$
Hamachi *et al.* (2001)	Membrane	Bentonite	Optical	10^{-7}	$\times 10^{-7}$
Li *et al.* (2003)	Membrane	Aqueous paper mill effluent	Ultrasound	10^{-8}	$\times 10^{-7}$

The Table also reports the method used to measure the growth rate. It is hard to find direct measurements of fouling layer growth rates due to the difficulties involved in measuring this quantity. It should be noted that cases where the reported growth rate is averaged over the duration of an experiment (those measured using volumetric, thickness or mass), these values are likely to be significantly lower than the initial values. Care must therefore be taken in cases where the average growth rate is close to the validity limit.

The Table shows that the majority of fouling types studied in the heat exchanger fouling community are associated with low deposit growth rates ($< 10^{-7}$ m/s). Thermal measurements of fouling in these systems are therefore expected to be free from the errors associated with heat transfer transients. They may be subject to errors associated with ageing, but this aspect is not explored further here. The interpretation of R_f-t data in the presence of ageing is discussed by Ishiyama *et al*. (2011). There is a shortage of quantitative studies of fouling subject to ageing for comparison with the SSA validity criterion.Exceptions to this general finding are found in studies of particulate fouling and crystallisation fouling.

Table 2 shows that particulate fouling is associated with the fastest growth rates as this process often occurs at conditions where there are high rates of reaction, heat and mass transfer. Particulate fouling often originates from combustion, such as waste incinerators (van Beek *et al.*, 2001) and coal-fired power plant (Bryers, 1996). The typical timescales in combustion are likely to be very short due to the high temperatures (Bott, 1987) and the use of large gas side velocities. These small timescales lead to fast growth rates for fouling layers.

Rapid crystallisation fouling also brings a further complicating factor, which is not considered here, namely the release (or absorption) of latent heat which accompanies the phase change. This is best considered by post-experimental calculation of the maximum heat flux associated with the maximum deposition rate and comparing this value with the rate of heat transfer by convection *etc*. at that point.

Particulate Fouling

Particulate fouling stands out in Table 2 as a process where thermal measurements may be unreliable owing to the high growth rates and low thermal diffusivities due to the presence of gases or vapours in the voids. Further evidence that the SSA may yield large errors in estimating particulate deposition rates by thermal measurements can be drawn from the experimental data on deposition in turbulent pipe flows in Figure 7 compiled by Young and Leeming (1977). The plot shows the relationship between the dimensionless deposition velocity, V_{dep+}, and the dimensionless particle relaxation time, τ_p. The latter parameter describes the extent to which the particles adhere to the flow streamlines. As the particles get larger they do not follow the streamlines and their motion is determined chiefly by their inertia.

The Figure shows that the maximum dimensionless deposition velocity is found in the inertia moderated regime, with $V_{dep+} \sim 0.1$. This result can be used to estimate a maximum growth rate. The dimensionless deposition velocity is defined as:

$$V_{dep+} = \frac{J_w}{C_m u*} \tag{16}$$

where J_w is the mass flux of material transported to the wall, C_m is the mass concentration of particles (mass of particles per unit volume) and $u*$ is the friction velocity.

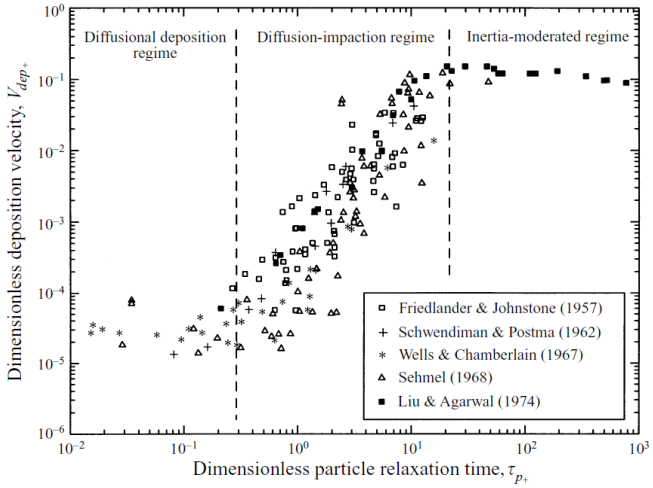

Fig. 7 Summary of experimental data reported for particle deposition from fully developed turbulent pipe flow. Reproduced from Young and Leeming (1997).

Assuming that all particles that hit the wall stick to the wall allows the maximum growth rate to be estimated from:

$$G = \frac{V_{dep+} C_m u^*}{\rho_f} = \frac{C_m u^*}{10 \rho_f} \qquad (17)$$

Van Beek *et al.* (2001) reported typical values of waste incinerator fouling layer bulk densities of 1300 kg/m^3. Assuming this value to be representative of particulate fouling scenarios allows the growth rate to be plotted as a function of the combined variable $C_m u^*$ in Figure 8. The locus shows that G reaches a value of 10^{-5} m/s when $C_m u^* \sim$ 0.2 kg m^{-2}s^{-1}. This corresponds to a friction velocity of 10 m/s and a solid density of 0.02 kg/m^3. It is noteworthy that the operating conditions employed in particle conveying and combustion processes often feature values of this order of magnitude or greater.

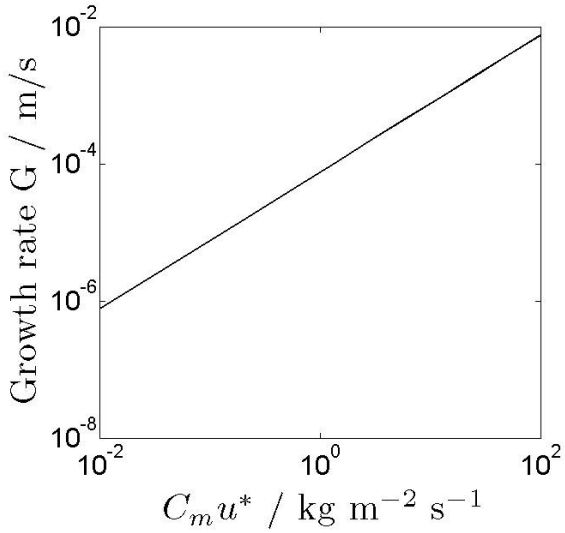

Fig. 8 Effect of the combined deposition variable [Equation 17] on the maximum particulate fouling rate.

This result indicates that care must be taken when considering thermal monitoring of particulate fouling in gaseous environments where the timescales can be very short. The particulate fouling studies cited in Table 2, those of Sathyanarayanarao Subbarao *et al.* (2011) and Kalisz *et al.* (2005), both employed non-thermal methods in their experiments so are not affected by this finding.

CONCLUSIONS

1. The common assumptions made in the monitoring of fouling layer thickness by thermal measurements, namely linear temperature profiles and instantaneous steady state, have been subjected to a critical quantitative analysis. The approach taken by Lister *et al.* (2012) shows this how this assumption can lead to a tractable error caused by the finite thermal inertia of the fouling layer.

2. The error in the steady state analysis was found to be strongly dependent upon the magnitude of the growth rate and the thermal diffusivity of the fouling layer. For hydrocarbon and aqueous liquids, the error becomes significant at deposit growth rates larger than 10^{-5} m/s. Extension of the analysis approach to deposits subject to ageing was demonstrated for a case with fixed temperature difference across the layer.

3. A study of fouling rates reported for different fouling types indicated that the steady state analysis was valid for most cases. Gas-side particulate fouling was identified as a process where the short timescales and high mass fluxes could lead to problems in interpreting thermal fouling data. A guideline for when the steady state analysis will yield large errors for particulate fouling (assuming perfect sticking) was identified as $C_m u^* = 0.2$ kg/m^{2}s.

ACKNOWLEDGEMENTS

A PhD studentship for V.Y. Lister from Huntsman is gratefully acknowledged.

NOMENCLATURE

Roman

a	Fouling layer thickness,	m
b	Coke layer thickness,	m
C_m	Particle concentration,	kg/m^3
G	Deposit growth rate,	m/s
g_A	Deposit growth rate parameter,	m/s$^{0.65}$
g_D	Ageing rate parameter,	m/s$^{0.5}$
h	Film heat transfer coefficient,	W/m^2 K
H	Scaled heat transfer coefficient, = h/k	1/m
J_w	Mass flux of particles to wall,	kg/m^2 s
k	Thermal conductivity,	W/m K
m_d	Thermal deposition rate factor,	W/m K s
n_r	Thermal removal rate factor,	1/s
R_f	Fouling layer thermal resistance,	m^2 K/W
$R_{f\infty}$	Asymptotic fouling resistance,	m^2 K/W
t	Time,	s
T	Temperature,	K
U	Overall heat transfer coefficient,	W/m^2 K
u^*	Friction velocity	m/s
V_{dep+}	Dim'less particle deposition velocity,	
x	Linear co-ordinate,	m

Greek

α	Thermal diffusivity,	m^2 / s
θ	Dimensionless temperature,	-
ρ_f	Deposit bulk density	kg/m
τ_p	Dimensionless particle relaxation time,	-

Subscript

a	Deposit-process stream interface
b	Bulk temperature
coke	Coke layer
est	Estimated
gel	Gel layer
w	Wall
0	Initial temperature

Superscript

S	Steady State
T	Transient

REFERENCES

van Beek, M.C., Rindt, C.C.M., Wijers, J.G. and van Steenhoven, A.A., (2001) Analysis of fouling in refuse waste incinerators, *Heat Transfer Eng.*, Vol. 22(1), pp. 22–31.

Bott, T.R. (1987) Gas side fouling, *Fouling Science and Technology*, eds. Melo, L.F., Bott, T.R. and Bernardo, C.A., pp. 191 -203.

Bryers, R.W. (1996) Fireside slagging, fouling and high temperature corrosion of heat-transfer surface due to impurities in steam-raising fuels, *Progr. Energy Combustion Sci.*, Vol. 22, pp. 29–120.

Characklis, W.G. (1981) Fouling biofilm development: a process analysis, *Biotech. Bioeng.*, Vol. 23, pp. 1923-1960.

Epstein, N. (1983) Thinking about fouling: a 5×5 matrix, *Heat Transfer Eng.*, Vol. 4, pp 43-56.

Griess, J. C., Savage, H. C., and English, J. L. (1964) Effect of heat flux on the corrosion of aluminum by water: Part IV., US Atomic Energy Commission Report, (ORNL-3541, Oak Ridge National Laboratory, Oak Ridge, Tennessee, February 1964).

Groberichter, D. and Stichlmair, J. (2003) Crystallization fouling in packed columns, *Chem. Eng. Res. Des.*, Vol. 81, pp. 68-73.

Hasson, D. and Zahavi, J. (1960) Mechanism of calcium sulfate scale deposition on heat transfer surfaces, *Ind. Eng. Chem. Fund,* Vol. 9(1), pp. 1-9.

Hamachi, M. and Mietton-Peuchot, M. (2001) Cake thickness measurement with an optical laser sensor, *Chem. Eng. Res. Des.*, Vol. 79, pp. 151-155.

Huang, J-Y., Chew, Y.M.J. and Wilson, D.I. (2012) A spinning disc study of fouling of cold heat transfer surfaces by gel formation from model food fat solutions, *J. Food Eng.*, Vol. 109, pp. 49-61.

Ishiyama, E.M., Coletti, F., Macchietto, S, Paterson, W.R. and Wilson, D.I. (2010) Impact of deposit ageing on thermal fouling: lumped parameter model. *AIChE J.,* Vol. 56(2), pp. 531–545.

Ishiyama, E.M, Paterson, W.R. and Wilson, D.I. (2011) Exploration of alternative models for the aging of fouling deposits, *AIChEJ*, Vol. 57(11), pp. 3199-3209.

Kalisz, S. and Pronobis, M. (2005) Investigations on fouling rate in convective bundles of coal-fired boilers in relation to optimization of sootblower operation, *Fuel***,** Vol. 84, pp. 927-937.

Kern, D.Q., Seaton, R.E., 1959, A theoretical analysis of thermal surface fouling, *British Chem. Eng*. Vol. 4(5), pp. 258-262.

Li, J., Hallbauer, D.K. and Sanderson R.D. (2003) 'Direct monitoring of membrane fouling and cleaning during ultrafiltration using a non-invasive ultrasonic technique, *J. Membrane Sci.*, Vol. 215, 33-52

Lister, V.Y., Davidson, J.F. and Wilson, D.I. (2012) Calculating thermal fouling resistances from dynamic heat transfer measurements, *Chem. Eng. Sci*., Vol. 84, pp. 772–780.

Mahato, B.K., Cha, C.Y. and Shemilt, L.W. (1980) Unsteady state mass transfer coefficients controlling steel pipe corrosion under isothermal flow conditions, *Corrosion Sci.*, Vol. 20, pp. 421-441.

Salley, B., Gordon, P.W., McCormick, A.J., Fisher, A.C. and Wilson, D.I. (2012) Characterising the structure of photosynthetic biofilms using fluid dynamic gauging, *Biofouling,* Vol. 28(2), pp. 159-173.

Sathyanarayanarao Subbarao, K.K., Rindt, C.C.M and van Steenhoven, A.A. (2011) Growth rates of dry particulate fouling under variable process conditions, Proceeding of International Conference on Heat Exchanger Fouling and Cleaning, Crete, 2011.

Taylor, W. (1969) Kinetics of deposit formation from hydrocarbons, *Ind. Eng. Chem. Prod. Res. Dev.*, Vol. 8(4), pp. 375-380.

Young, J. and Leeming A. (1997) A theory of particle deposition in turbulent pipe flow, *J. Fluid Mech.*, Vol. 340, pp. 129-159.